TÜBİTAK

Turkish Journal of Chemistry

http://journals.tubitak.gov.tr/chem/

Research Article

Turk J Chem
(2019) 43: 520 – 530
© TÜBİTAK
doi:10.3906/kim-1807-44

Pore length- and ion concentration-dependent ionic current in cylindrical nanopores: an atomistic molecular dynamics study

Nazar İLERİ ERCAN*
Department of Chemical Engineering, Faculty of Engineering, Boğaziçi University, İstanbul, Turkey

Received: 11.07.2018 • **Accepted/Published Online:** 24.12.2018 • **Final Version:** 03.04.2019

Abstract: The sensing of individual molecules as they pass through nanopores under an external field is a popular research field. The approach is simply based on the detectable temporary blockades in the ionic current as the molecules pass through the nanopores. These signatures of the current have been shown to be a function of nanoparticle and nanopore size and geometry as well as the external electric field. However, models developed in this context fail to predict the experimentally observed behavior in technologically important shorter nanopores. Here we present atomistic molecular dynamics simulation results from colloidal nanoparticle translocation through mid-to-low aspect ratio charged nanopores under an external field. We show that not only the pore length but also the ion concentration of the media and the nanoparticle charge have important effects on the ionic current.

Key words: Molecular dynamics, nanoparticle translocation, ion current

1. Introduction

A detailed understanding of molecule translocation through pores or channels can provide critical improvements in fields including DNA sequencing,[1] sensing,[2] proteomics,[3] gene therapy,[4] and controlled drug delivery,[5] where efficient separation and identification of molecules is required. Indeed, pore-based separation, identification, and detection of particles is primarily derived from the working principle of Coulter counter, a device first introduced by R. H. Coulter to count the biological cells as they pass through micron-scale holes.[6] In brief, as the molecule passes through the pore under an external electric field, the ionic current decreases drastically (Figure 1) and hence, the pore is considered to be blocked temporarily due to the displacement of the salt solution by the molecule and hence resistance change in the pore. Once the molecule exits the pore, the current is restored to its initial open pore current value, which scales with the ion mobility, pore geometry, and applied voltage by:[7]

$$\boldsymbol{I \approx [(n\mu)_{K^+} + (n\mu)_{Cl^-}]\,\frac{D^2}{L}V}$$

where $\boldsymbol{n}$ and $\boldsymbol{\mu}$ are the ion density and the mobility, respectively, $\boldsymbol{D}$ is the diameter of the nanopore, $\boldsymbol{L}$ is the length of the nanopore, and V is the applied voltage. The pulse, i.e. the current change, caused by lower effective volume during the particle passage through the pore, is proportional to the volume of the sensed molecule and provides information on the particle size. The time interval between the current blockades and the

*Correspondence: nazar.ileri@boun.edu.tr

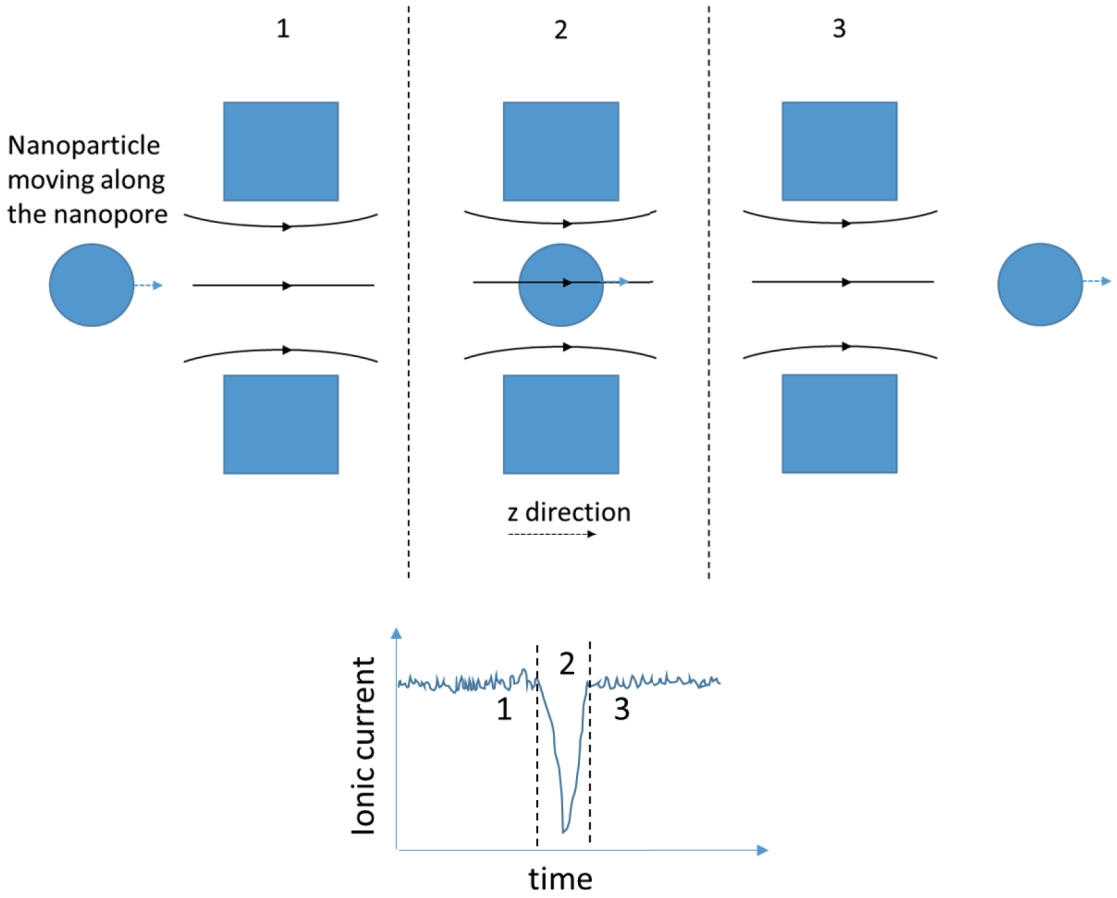

Figure 1. Schematic of a nanoparticle translocation through a nanopore and the corresponding current trace. 1: nanoparticle entering the nanopore, 2: nanoparticle passing through the nanopore, 3: nanoparticle exiting the nanopore.

time length of the blockade are the other parameters that provide the information on the particle concentration and dynamics, respectively.

Making use of the Coulter counter principle, several groups have studied the translocation of colloidal,[8–9] or biological objects such as polymers,[10] cells,[11] viral particles,[12] DNA,[13–15] RNA,[16] polymers/proteins,[17–19] and investigated the effects of particle size, concentration dynamics, charge density, external voltage,[8] as well as pore/channel size, geometry, and surface charge density. However, experimental results may sometimes be contradictory and not sufficient alone to provide the required resolution for a mechanistic understanding. For example, the magnitude of ionic current blockades has been unexpectedly shown to decrease in low aspect ratio pores with no clear understanding being provided.[9] Molecular dynamics simulations, in this context, can support the experiments by providing the information at molecular resolution. To date, molecular simulations have been employed in several studies to understand the transport properties through nanopores.[19–23] However, studies of atomic-scale simulations of colloidal nanoparticles through nanopores under an external field have been limited due to limited time and length scales attainable by these simulations.

Here we investigate in mid-to-low aspect ratio nanopores the effect of pore length and ionic strength on ion distributions and hence ionic current blockades by atomistic molecular dynamics (MD) simulations. We show that as the length of nanopore decreases the difference in the open and blocked states of current signatures

becomes less evident. We also demonstrate that ionic strength of the media can considerably change the current response upon pore blockages.

2. Results and discussion

2.1. Effects of pore length and ion concentration

To investigate the effect of pore length on ionic current, nanopores with different aspect ratio (length/diameter) in the range of 0.05–0.5 have been studied. Pore length (L), pore diameter (D), and nanoparticle diameter (D_{C60}) are selected such that their ratios are in the experimentally investigated range.[9] To minimize the effects of carbon nanotube (CNT) on the exclusion of ions.[24] and the internal structure of the fluid,[25] a (30, 30) single-walled carbon nanotube (SWCNT) is used. Although uncharged CNT is hydrophobic in nature, charged CNT under electric field becomes hydrophilic.[26] Three different conditions are considered for each nanopore length where the system contains: (a) no nanoparticle (C60), (b) C60 placed at the pore mouth, and (c) C60 placed at the center of the nanopore (Figure 2). Under experimental conditions the translocation of a nanoparticle through a nanopore has been shown to last for several hundreds of microseconds.[9] Therefore, in the simulations, the nanoparticle is held fixed at its position considering the short simulation times accessible to atomistic MD.

Figure 3 shows the density distributions of ions, water, K^+, and Cl^- along the nanopore length at low (0.11 M) KCl concentration. Here both the nanopore and the nanoparticle are negatively charged and a positive potential is applied. In general, high density of ions and water molecules are observed near membrane walls since the walls are charged and hydrophilic (Figures 3a and 3b). However, the charge density of water near membrane walls is much higher in shorter pores (aspect ratio $\leq$ 0.1) than longer pores, which is attributed to different hydration behavior of single and multigraphene layers.[27–28] As the nanopore length increases, the separation distance between the graphene walls increases and the wall behaves like a single graphene layer. Inside the nanopore, the ion density increases as the length of the nanopore increases (Figure 3c), which may be because of the ionic crowding, as longer nanopores have been shown to have higher pore resistance and lower pore conductance values.[29] When the nanoparticle is fixed at the center of the nanopore, an increase in ion density and a decrease in water density (Figure 3d) is observed at the center of the nanopore because of the attraction of charges to the negative C60 and the displacement of water molecules by C60, respectively. Similarly, Cl^- distributions decrease and K^+ distributions increase when C60 is placed at the center of the nanopore compared to the systems with no C60 (Figures 3e and 3f). Overall, cation distributions have the same trend with total ion distributions, i.e. as length increases ion density increases. However, for Cl^-, a plateau is observed in the density distributions for 0.1 and 0.2 aspect ratio nanopores followed by an increase for 0.05 aspect ratio nanopore, which indicates negligible wall effects in the lower aspect nanopores.

At high (1.1 M) salt concentration, different from the trend observed with low KCl concentration, at all studied nanopore lengths, ion density distributions inside the nanopore when C60 is at the center become less than those of nanopores without C60 (Figure 4a). A reduction in ion density may in general represent a drop (negative peak) in the ionic current, while an increase may indicate an enhancement (positive peak) in the current. Experimentally, such a dependence of current blockades on ion concentration has been reported by several groups.[30–32] Inside the nanopore, even though a nanoparticle causes the displacement of ions, at low ion concentrations highly charged nanoparticles surrounded by counterions may increase the transport of ions due to the low screening effects. On the other hand, water and Cl^- density profiles follow the same trend as with low ion concentrations, i.e. water densities decrease and Cl^- densities increase with increasing pore length

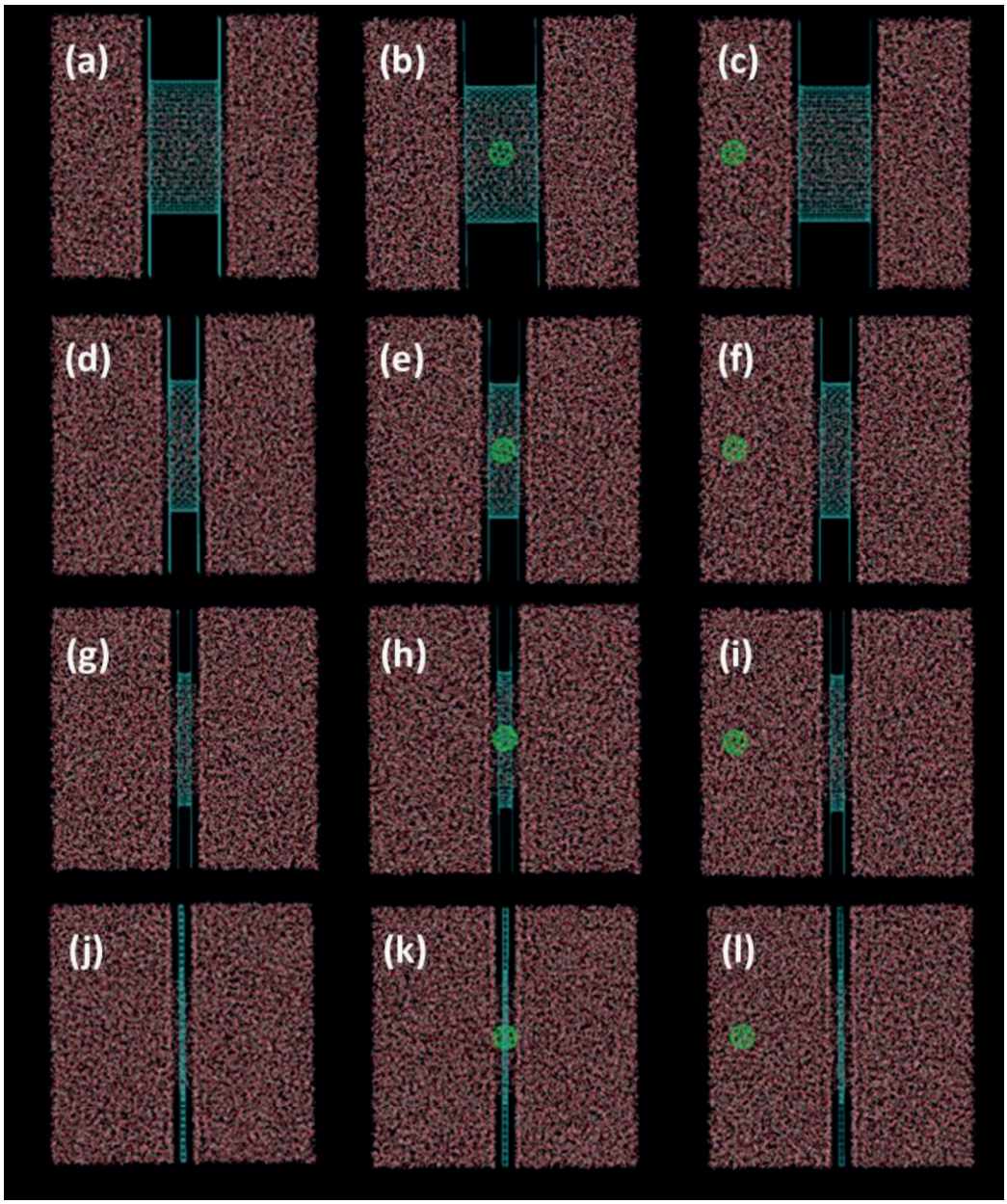

Figure 2. Studied pore configurations: (a–c) 2 nm, (d–f) 0.8 nm, (g–i) 0.4 nm, (j–l) 0.2 nm pore length.

(Figures 4b and 4c). However, due to the high ion concentrations and hence displacement of water molecules by the ions, slightly lower water densities and higher Cl^- and K^+ densities are obtained inside the pore compared to the low ion concentration profiles. Furthermore, K^+ densities inside the nanopore increase with increasing pore length (Figure 4d), but similar density distributions are observed for the same length pore configurations irrespective of nanoparticle existence or location. At high ionic concentration, a saturation point for counterions can be easily reached diminishing the effect of K^+ on the overall ion density distributions. No major difference is detected in the density profiles of configurations with no C60 and with C60 at the pore mouth by both ion concentrations.

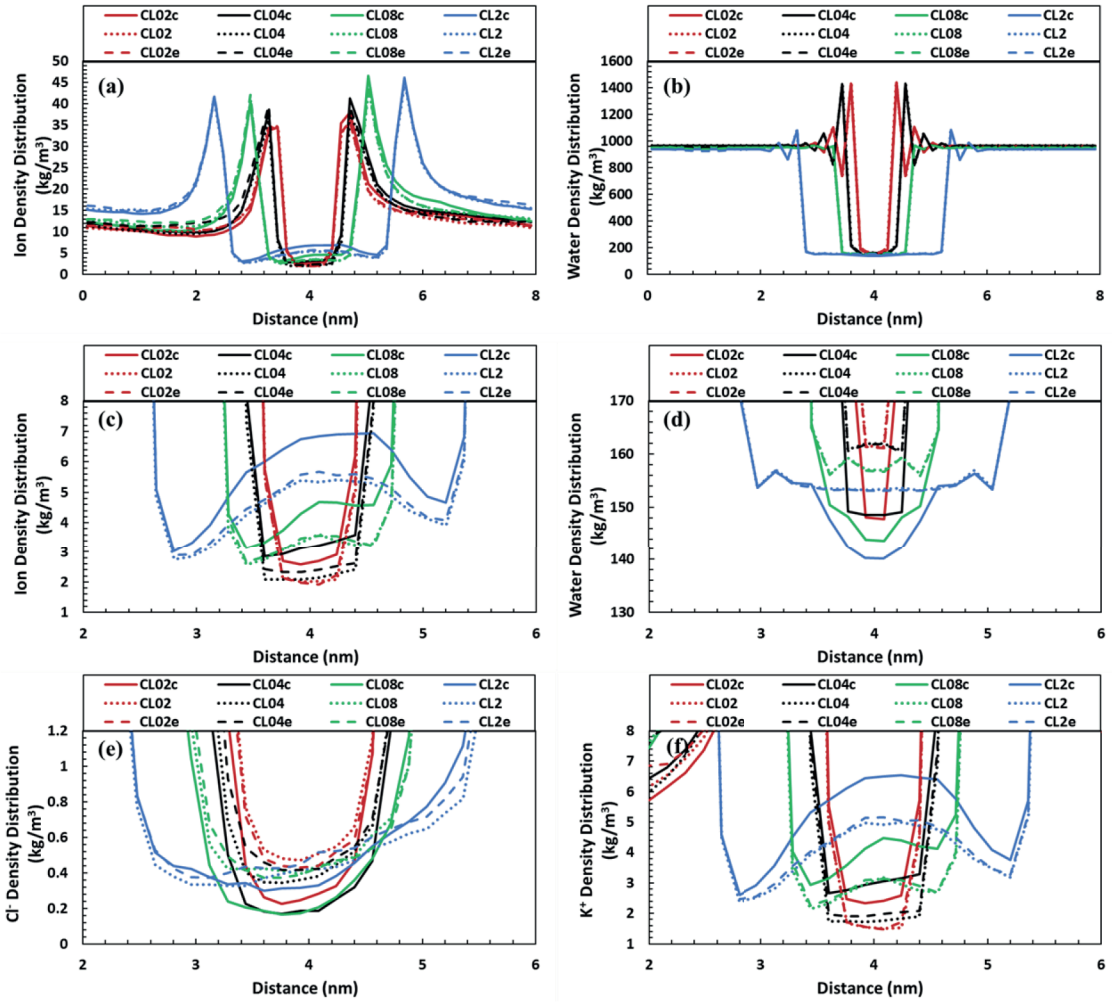

Figure 3. Density distributions of ions (a,c), water molecules (b,d), Cl^- (e), and K^+ (f) along pore length (z direction) using 0.11 M KCl concentration under 100 mV/nm electric field. (c) and (d) are enlarged images of (a) and (b), respectively. Both nanopore and nanoparticle are negatively charged. CLx, CLxc, and CLxe stand for cylindrical pores with no nanoparticle in the system, cylindrical pores with nanoparticle centered inside the nanopore, and cylindrical pores with nanoparticle placed at the pore mouth, respectively, where x: 02, 04, 08, 2 represent the studied pore length (i.e. 0.2 nm, 0.4 nm, 0.8 nm, 2 nm, respectively). In general, K^+ and hence total ion densities increase whereas water and Cl^- densities decrease when nanoparticle is placed at the center of the nanopore compared to the systems with no nanoparticle.

Figure 5 shows ion and water radial distribution functions (RDFs) with respect to the center of mass (COM) of the nanopore around axes parallel to z-axis (i.e. only in x-y plane). At low KCl concentration, ion ordering near pore walls becomes important in pores with an aspect ratio of 0.5 (Figure 5a), whereas at high KCl concentration, nearly uniform distributions of ions are obtained inside the nanopores, yet still with higher RDF values for 0.5 aspect ratio pores (Figure 5b). Water ordering around nanopore walls, however, increases with increasing pore length, but does not show apparent variation with ion concentration except for ~ 2% increase in the peak values (Figures 5c and 5d). Placement of the nanoparticle into the simulation box has no major effect on the ordering of ions except for the appearance of a shallow valley at the pore center due the excluded volume, but a slight increase in the ordering of water molecules (appearance of the 1^{st} peak from

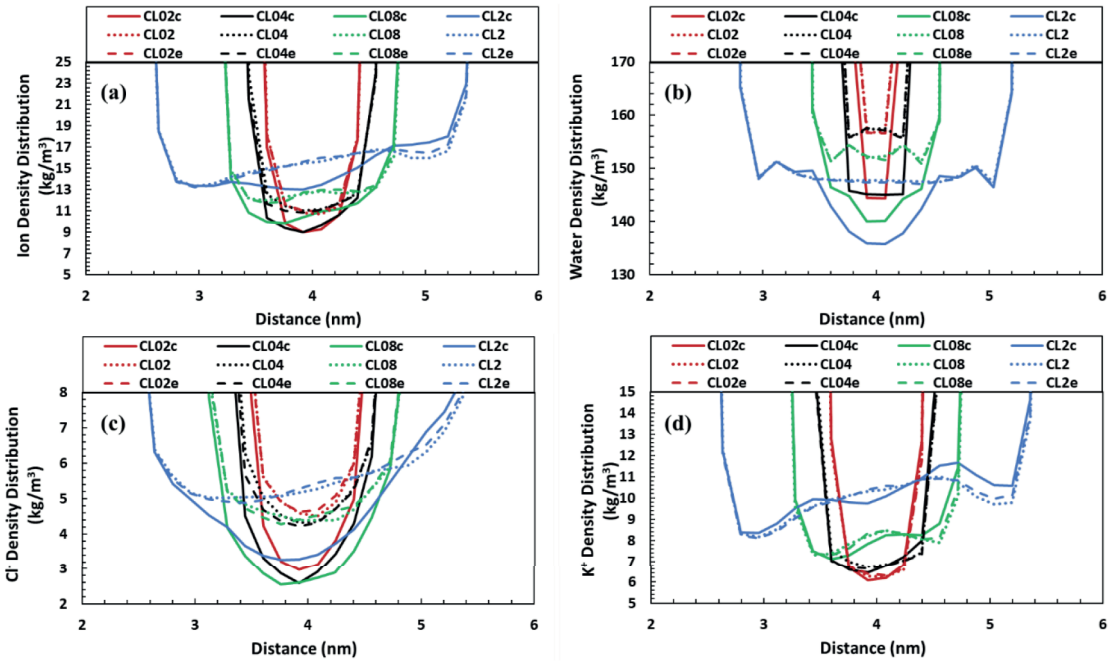

Figure 4. Density distributions of ions (a), water molecules (b), Cl^- (c), and K^+ (d) along pore length (z direction) using 1.1 M KCl concentration. Enlarged images are given for a better representation. Both nanopore and nanoparticle are negatively charged. CLx, CLxc, and CLxe stand for cylindrical pores with no nanoparticle in the system, cylindrical pores with nanoparticle centered inside the nanopore, and cylindrical pores with nanoparticle placed at the pore mouth, respectively, where x: 02, 04, 08, 2 represent the studied pore length (i.e. 0.2 nm, 0.4 nm, 0.8 nm, 2 nm, respectively). In general, lower K^+, CL^-, and hence total ion densities and lower water densities are obtained along the nanopore when nanoparticle is placed at the center of the nanopore compared to the systems with no nanoparticle.

the pore center in addition to a more distinct valley at the pore center in the RDF plots) is observed resulting from the hydration of C60. No clear difference is seen in 2D-RDFs of solvent with respect to pore center when C60 is placed at the pore mouth and the pore center (Figures 5c and 5d insets), which is attributed to the close placement of C60 to the pore mouth. Ion ordering around C60, on the other hand, increases and the peak values shift to right slightly with increasing pore length when C60 is fixed at the center of the pore at low KCl concentration (Figure 6a). At the lowest investigated aspect ratio (0.05), the ordering approaches to that of a C60 in bulk salt solution at 0.11 M indicating negligible wall/confinement effects. When C60 is placed at the pore mouth, RDF values become less with more even distributions than that of C60 in bulk solution due to the attraction by the membrane walls. At higher salt concentrations, however, the RDF values are all larger than the RDF of C60 in bulk at 1.1 M KCl solution (Figure 6b). Ion ordering around C60 is less affected by the membrane walls, since at high ionic strength the ions are more closely and hence strongly attracted to C60 surface. The RDF values increase with increasing pore length and greater ordering is observed when C60 is placed at the center of the nanopore due to the confinement effect.

Assuming high KCl concentrations yield in negative peaks in the ionic current, we have calculated the change in the ionic current as well as the change in the total number of ions inside the nanopore when there is no C60 and when C60 is fixed at the pore center (Table). In agreement with the experimental findings, a decrease in the ionic current change is observed with decreasing aspect ratio pores except for the nanopore with an aspect ratio of 0.05, where the current blockade behavior is reversed and a positive peak is obtained.

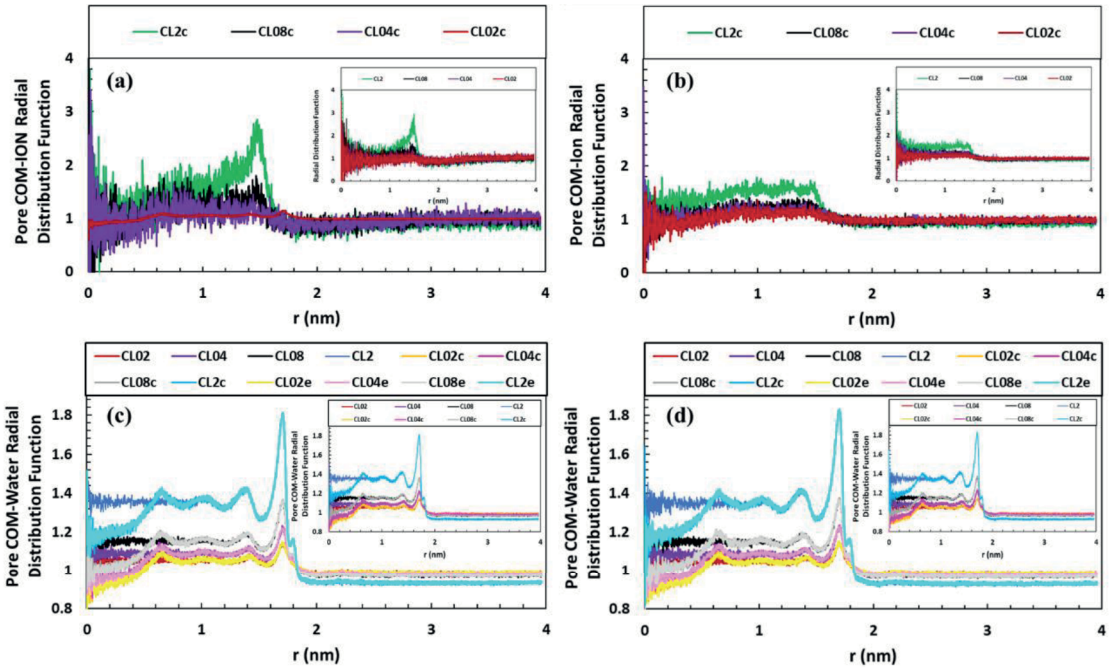

Figure 5. Pore COM-ion (a,b) and pore COM-water (c,d) radial distribution functions with respect to radial distance in xy-plane using 0.11 M (a,c) and 1.1 M (b,d) KCl concentrations. Both nanopore and nanoparticle are negatively charged. CLx, CLxc, and CLxe stand for cylindrical pores with no nanoparticle in the system, cylindrical pores with nanoparticle centered inside the nanopore, and cylindrical pores with nanoparticle placed at the pore mouth, respectively, where x: 02, 04, 08, 2 represent the studied pore length (i.e. 0.2 nm, 0.4 nm, 0.8 nm, 2 nm, respectively). Insets in (c,d) are the corresponding pore COM-water radial distribution functions for CLx and CLxc, given for a better comparison. Structuring of ions and water near pore walls becomes more significant with increasing pore length. Increasing ionic concentration decrease the ordering of ions.

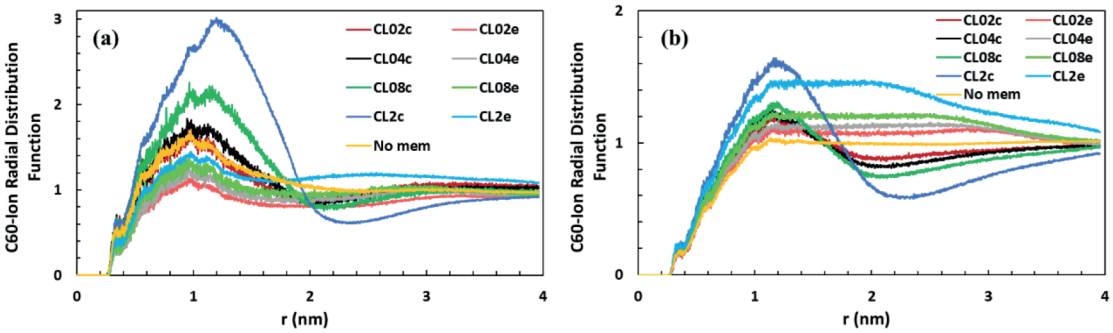

Figure 6. C60-ion radial distribution functions with respect to radial distance using 0.11 M (a) and 1.1 M (b) KCl concentrations. Both nanopore and nanoparticle are negatively charged. CLx, CLxc, and CLxe stand for cylindrical pores with no nanoparticle in the system, cylindrical pores with nanoparticle centered inside the nanopore, and cylindrical pores with nanoparticle placed at the pore mouth, respectively, where x: 02, 04, 08, 2 represent the studied pore length (i.e. 0.2 nm, 0.4 nm, 0.8 nm, 2 nm, respectively). No mem stands for simulations of C60 in KCl solution excluding the presence of a membrane. Ion ordering around C60 increases with increasing pore length and when C60 is placed at the center of nanopore.

Conversely, the change in the average total number of ions inside the nanopore per pore length increases in general with decreasing pore length, yet this change is rather small in 0.05–0.2 aspect ratio nanopores. That is, the displacement of ions increases with decreasing pore length up to a length beyond which ion displacement does

not show any major variation. Moreover, a reduction in the pore length also reduces the wall and confinement effects of the pore which may reduce the residence times of the ions inside the pore and hence increase their velocity. Indeed, the density distribution profiles, and the radial distribution profiles of ions around C60 and pore walls given above points to the similar or reducing confinement and structuring of ions in $\leq$0.2 aspect ratio pores. Consequently, the combined effect of reaching a saturation point for ion displacement together with similar or diminishing wall/confinement effects lead to the increased ion velocities and hence amplified current values (shallow peak minima) in the blocked state, which in general results in a decline in % current changes upon blockades with decreasing pore length.

Table. The change in ionic current and average total number of ions inside the nanopore when C60 is placed at the center of a nanopore. KCl concentration and electric field are 1.1 M and 100 mV, respectively. Both the nanopore and the nanoparticle are negatively charged.

	Time-averaged ionic current e/ps			Average total number of ions inside the nanopore/pore length		
	No C60	C60 at the center	% change	No C60	C60 at the center	% change
CL2	0.0070	–0.0350	589.2	15.93	14.80	7.1
CL08	0.0413	–0.0365	188.4	11.01	9.39	14.8
CL04	0.0404	–0.0053	113.2	11.63	9.85	15.3
CL02	–0.0185	0.1079	–682.4	10.78	8.94	17.0

2.2. Effect of nanoparticle charge

A positively charged (+)-C60 at low KCl concentration results in the ion density profiles similar to those of negatively charged (-)-C60 at high KCl concentration, that is the ion density inside the nanopore decreases when C60 is fixed at the center compared to the no C60 configurations (Figure 7a). In this density difference K^+ plays a dominant role, as (+)-C60 attracts Cl^- and repels K^+. The pore length dependent behavior of ion density distribution is the same as in the previous cases, where the ion density increases with increasing pore length. In addition, the water density profiles along the pore length are also similar to those of (-)-C60 at 0.11 M KCl concentration (Figure 7b). Figure 7c demonstrates the RDFs of ions around (+)-C60 in the presence of 0.05 and 0.5 aspect ratio nanopores compared with (-)-C60 profiles. Although similar RDF profiles are obtained for positively and negatively charged nanoparticles when the C60 is placed at the pore mouth, less structuring of ions and a greater spacing of ions from the C60 surface are observed with (+)-C60 when the nanoparticle is centered inside the pore, which is attributed to the charge penalty induced by oppositely charged nanopore and nanoparticle counterions.

2.3. Conclusion

In this study, we have shown that the ion current signatures are highly dependent on the aspect ratio of the nanopore, the ionic strength of the media, and the charge of the translocating nanoparticle. At low KCl concentration, higher ion density values are obtained when C60 is at the center of the nanopore indicative of positive peaks upon current blockades, whereas a reverse behavior is attained at high KCl concentration or when C60 is oppositely charged. The structuring of ions around the nanopore and the nanoparticle becomes significant with decreasing ionic concentration and when both the pore and the nanoparticle bear the same

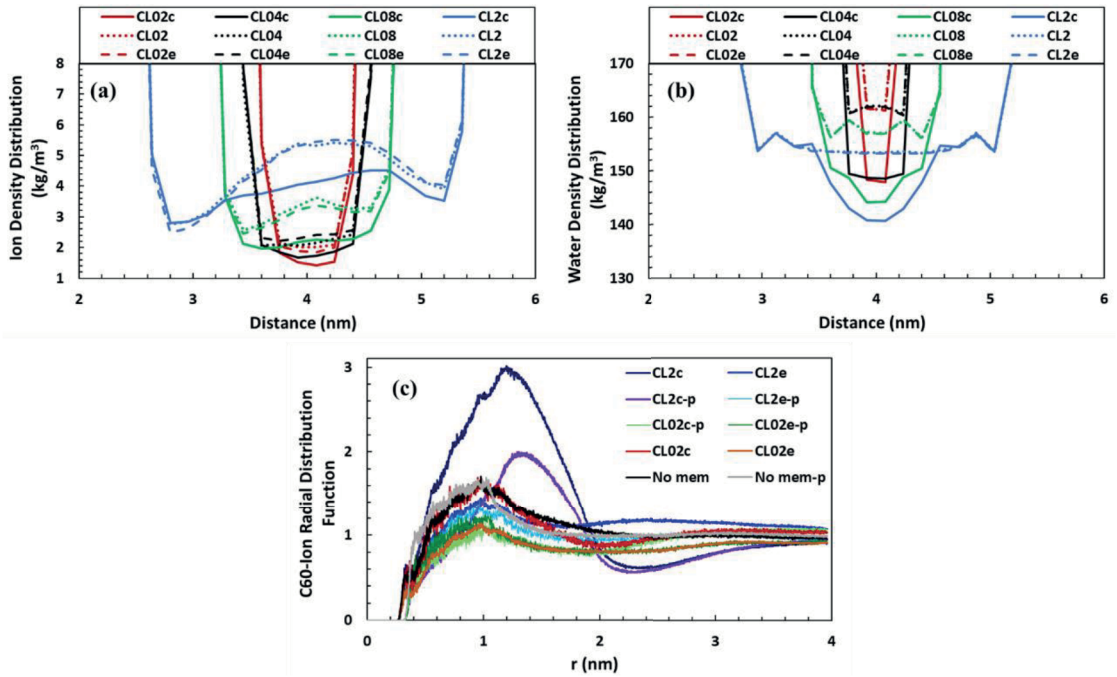

Figure 7. Enlarged images of (a) ion and (b) water density distributions along pore length (z direction) using 0.11 M KCl and positively charged C60. (c) Comparison of C60-ion radial distribution functions with respect to radial distance for positively and negatively charged nanoparticles. CLx, CLxc(-p), and CLxe(-p) stand for cylindrical pores with no nanoparticle in the system, cylindrical pores with nanoparticle centered inside the nanopore, and cylindrical pores with nanoparticle placed at the pore mouth, respectively, where x: 02, 04, 08, 2 represent the studied pore length (i.e. 0.2 nm, 0.4 nm, 0.8 nm, 2 nm, respectively) and –p stands for positively charged C60. In general, lower ion densities are obtained inside the pore when nanoparticle is placed at the center of the nanopore compared to the systems with no nanoparticle. Ions are more largely spaced from the nanoparticle and ordering becomes less significant for positive C60 compared with negative C60.

charge sign. In agreement with the experimental findings, a decrease in the change of ionic current between open and blocked states are observed with decreasing aspect ratio of the nanopore which is attributed to a very small change of ion displacement values above a threshold length together with an increase in ion velocities upon reduced confinement effects. The findings of this research provide an insight on the design of pore-based sensors for enhanced performances.

3. Experimental

Nanoporous membrane is composed of a (30, 30) type SWCNT embedded in between two graphite sheets having a 4 nm hole at the center. The diameter of the nanopore is 4 nm and the length ranges between 0.2 and 2 nm. The membrane is held fixed at the center of an 8 nm × 8 nm × 8 nm periodic simulation box where it divides the box into two equal compartments. To mimic the experimental conditions the surface charge density of the membrane is set to approximately –0.4 e/nm^2.[33] Water and ions are explicitly introduced to the simulation box. The concentration of salt is set to 0.11 M or 1.1 M KCl representing low and high concentrations of salt solutions, respectively. The nanoparticle, having a topological diameter of 0.7 nm, is modeled by C60. The surface charge density of the nanoparticle is set to ± 0.5 e/nm^2 being in the range of the experimentally reported values.[34] Counterions are presented to the simulation box to make the overall system charge neutral.

An external electric field of 100 mV/nm along +z direction is applied to the system.

MD simulations are performed with the Gromacs 5.1.1.[35] simulation package in an NVT ensemble, where the number of particles (N) and the volume (V) are kept constant for a given temperature T. The OPLS-AA force-field.[36] with the TIP4P water model.[37] was used with a time step of 2 ps, and Verlet cut-off scheme.[38−39] with a cut-off distance of 1.0 nm. The van der Waals cut-off was set to 1.0 nm. Long range electrostatic interactions were calculated using the particle-mesh Ewald method.[40−41] A fourth order interpolation, 0.12 nm grid spacing, and 1.0 nm cut-off in real space was applied. Long range dispersion corrections were applied for energy. Temperature was set to 300 K and controlled by the Nosé–Hoover thermostat.[42−43] with a coupling time of 0.4 ps. All simulations were energy minimized using the steepest method, then equilibrated in the absence of electric field for 10 ns before the production runs. Production runs were performed for 100 ns with properties calculated by block averaging over the last 80 ns. Visual MD.[44] was used for the visualization of the simulation evolution over time. To calculate the average total number of ions inside the nanopore and hence the ionic current, velocity and coordinate information was extracted from the trajectory files. Using the gathered information, the time-averaged ionic current was calculated through $[ERR : md : MbegChr = 0x2329, MendChr = 0x232A, nParams = 1]_t$, where q and v_z are the charge and the axial velocity of the ion, respectively, and L is the length of the nanopore.

Acknowledgments

This work was supported by the Scientific and Technological Research Council of Turkey (TÜBİTAK), Grant No: 116C065. Computations were performed at TÜBİTAK ULAKBİM, High Performance and Grid Computing Center (TRUBA resources).

References

1. Branton, D.; Deamer, D. W.; Marziali, A.; Bayley, H.; Benner, S. A.; Butler, T.; Di Ventra, M.; Garaj, S.; Hibbs, A.; Huang, X.; et al. *Nat. Biotechnol.* **2008**, *26*, 1146-53.
2. Lin, X.; Ivanov, A. P.; Edel, J. B. *Chem. Sci.* **2017**, *8*, 3905-3912.
3. Issaq, H. J. *Electrophoresis.* **2001**, *22*, 3629-38.
4. Franceschini, L.; Soskine, M.; Biesemans, A.; Maglia, G. *Nat. Commun.* **2013**, *4*, 2415.
5. Slowing, I. I.; Vivero-Escoto, J. L.; Wu, C.-W.; Lin, V. S. Y. *Adv. Drug Deliv. Rev.* **2008**, *60*, 1278-1288.
6. Coulter, W. B. U. S. patent 2, 656, 508, 1953.
7. Sattler, K. D. *Handbook of nanophysics: nanomedicine and nanorobotics*; CRC Press: Boca Raton, Florida, USA, 2010.
8. Bacri, L.; Oukhaled, A.; Schiedt, B.; Patriarche, G.; Bourhis, E.; Gierak, J.; Pelta, J.; Auvray, L. *J. Phys. Chem. B.* **2011**, *115*, 2890-2898.
9. Davenport, M.; Healy, K.; Pevarnik, M.; Teslich, N.; Cabrini, S.; Morrison, A. P.; Siwy, Z. S.; Le tant, S. E. *ACS Nano.* **2012**, *6*, 8366-8380.
10. Luo, K.; Huopaniemi, I.; Ala-Nissila, T.; Ying, S.-C. *J. Chem. Phys.* **2006**, *124*, 114704.
11. Asghar, W.; Wan, Y.; Ilyas, A.; Bachoo, R.; Kim, Y.-t.; Iqbal, S. M. *Lab chip.* **2012**, *12*, 2345-2352.
12. Zhou, K.; Li, L.; Tan, Z.; Zlotnick, A.; Jacobson, S. C. *J.Am. Chem. Soc.* **2011**, *133*, 1618-1621.
13. Aksimentiev, A.; Heng, J. B.; Timp, G.; Schulten, K. *Biophys. J.* **2004**, *87*, 2086-2097.
14. Aksimentiev, A. *Nanoscale.* **2010**, *2*, 468-483.

15. Storm, A. J.; Storm, C.; Chen, J.; Zandbergen, H.; Joanny, J.-F.; Dekker, C. *Nano Lett.* **2005**, *5*, 1193-1197.
16. Butler, T. Z.; Gundlach, J. H.; Troll, M. A. *Biophys. J.* **2006**, *90*, 190-199.
17. Yusko, E. C.; Johnson, J. M.; Majd, S.; Prangkio, P.; Rollings, R. C.; Li, J.; Yang, J.; Mayer, M. *Nat. Nanotechnol.* **2011**, *6*, 253-260.
18. Fologea, D.; Ledden, B.; McNabb, D. S.; Li, J. *Appl. Phys. Lett.* **2007**, *91*, 053901.
19. Nikoofard, N.; Fazli, H. *Phys. Rev. E.* **2012**, *85*, 021804.
20. Garaj, S.; Hubbard, W.; Reina, A.; Kong, J.; Branton, D.; Golovchenko, J. *Nature.* **2010**, *467*, 190.
21. Ai, Y.; Qian, S. *Phys. Chem. Chem. Phys.* **2011**, *13*, 4060-4071.
22. Nadtochiy, A.; Melnikov, D.; Gracheva, M. *ACS Nano.* **2013**, *7*, 7053-7061.
23. Jou, I. A.; Melnikov, D. V.; Gracheva, M. E. *Nanotechnology.* **2016**, *27*, 205201.
24. Fornasiero, F.; Park, H. G.; Holt, J. K.; Stadermann, M.; Grigoropoulos, C. P.; Noy, A.; Bakajin, O. *Proc. Natl. Acad. of Sci. U. S. A.* **2008**, *105*, 17250-17255.
25. Alexiadis, A.; Kassinos, S. *Chem. Eng. Sci.* **2008**, *63*, 2047-2056.
26. Huang, B.; Xia, Y.; Zhao, M.; Li, F.; Liu, X.; Ji, Y.; Song, C. *J. Chem. Phys.* **2005**, *122*, 084708.
27. Wang, S.; Zhang, Y.; Abidi, N.; Cabrales, L. *Langmuir.* **2009**, *25*, 11078-11081.
28. Dai, J.-F.; Wang, G.-J.; Ma, L.; Wu, C.-K. *Rev. Adv. Mater. Sci.* **2015**, *40*, 60-71.
29. Kant, K.; Priest, C.; Shapter, J. G.; Losic, D. *Sensors.* **2014**, *14*, 21316-21328.
30. Smeets, R. M.; Keyser, U. F.; Krapf, D.; Wu, M.-Y.; Dekker, N. H.; Dekker, C. *Nano Lett.* **2006**, *6*, 89-95.
31. Chang, H.; Kosari, F.; Andreadakis, G.; Alam, M.; Vasmatzis, G.; Bashir, R. *Nano Lett.* **2004,** *4*, 1551-1556.
32. Fan, R.; Karnik, R.; Yue, M.; Li, D.; Majumdar, A.; Yang, P. *Nano Lett.* **2005**, *5*, 1633-1637.
33. Galla, L.; Meyer, A. J.; Spiering, A.; Sischka, A.; Mayer, M.; Hall, A. R.; Reimann, P.; Anselmetti, D. *Nano Lett.* **2014**, *14*, 4176-4182.
34. Barisik, M.; Atalay, S.; Beskok, A.; Qian, S. *J. Phys. Chem. C.* **2014**, *118*, 1836-1842.
35. Abraham, M. J.; Murtola, T.; Schulz, R.; Páll, S.; Smith, J. C.; Hess, B.; Lindahl, E. *SoftwareX.* **2015**, *1*, 19-25.
36. Tieleman, D. P.; MacCallum, J. L.; Ash, W. L.; Kandt, C.; Xu, Z.; Monticelli, L. *J. Phys-Condens. Mat.* **2006**, *18*, S1221.
37. Jorgensen, W. L.; Chandrasekhar, J.; Madura, J. D.; Impey, R. W.; Klein, M. L. *J. Chem. Phys.* **1983**, *79*, 926-935.
38. Verlet, L. *Phys. Rev.* **1967**, *159*, 98-103.
39. Páll, S.; Hess, B. *Comput. Phys. Commun.* **2013**, *184*, 2641-2650.
40. Darden, T.; York, D.; Pedersen, L. *J. Chem. Phys.* **1993**, *98*, 10089-10092.
41. Essmann, U.; Perera, L.; Berkowitz, M. L.; Darden, T.; Lee, H.; Pedersen, L. G. *J. Chem. Phys.* **1995**, *103*, 8577-8593.
42. Nosé, S. *Mol. Phys.* **1984**, *52*, 255-268.
43. Hoover, W. G. *Phys. Rev. A*. **1985**, *31*, 1695.
44. Humphrey, W.; Dalke, A.; Schulten, K. *J. Mol. Graph.* **1996**, *14*, 33-38.